PCCP

ROYAL SOCIETY OF CHEMISTRY

PAPER

View Article Online
View Journal | View Issue

Cite this: *Phys. Chem. Chem. Phys.*, 2025, **27**, 24061

Delving into multiple ionization of nitromethane using $\omega/2\omega$ fs laser fields

Panagiotis Vamvakidis and Constantine Kosmidis *

Received 30th September 2025,
Accepted 23rd October 2025

DOI: 10.1039/d5cp03775a

rsc.li/pccp

We report on the multiple ionization of nitromethane in the near IR region. Based on experiments using linearly and circularly polarized beams, we conclude that the nitromethane dications and tricications that ultimately fragment *via* direct cleavage of the C–N bond are generated by a rescattering process. From the kinetic energies of the ionic fragments and their dependence on the relative phase of the laser fields that constitute an $\omega/2\omega$ fs asymmetric field, the main dissociation channels have been accurately identified. The existence of at least three nitromethane isomers has been verified by the recorded mass spectra. By the combined study of the deuterated isotopologue, a dissociation channel in the dication that could result in an asymmetric charge distribution is discussed. The characteristics of this channel depend on the laser field intensity. At higher laser intensities, a contribution in the double ionization from HOMO−1 is also detected. This is imprinted by a drastic change in the dependence of the ionic fragments on the phase of the asymmetric field, which highlights the possibilities offered using $\omega/2\omega$ fs fields.

Introduction

Nitro compounds belong to a broad family of highly active and energetic molecules due to the presence of one or more nitro groups ($-NO_2$).[1,2] Nitromethane (CH_3NO_2) is the simplest nitroalkane and has been the subject of extensive theoretical and experimental investigation.[3–7] Understanding the photochemistry and dissociation dynamics of nitromethane is essential because of its significance in detonation processes,[4] combustion,[5] industrial and atmospheric chemistry.[6] Different experimental techniques were used to study the dissociation processes in depth.[1–4,6–11] Among these, photoexcitation is an effective experimental approach to gain more insight into the dissociation of nitromethane.[12–16] Laser excitation at selective wavelengths[4,6–9] has revealed a complex intramolecular transformation, while ultrashort and strong laser beams[3,10,11] offer the ability to study the fragmentation dynamics and the dissociation from multiply charged ionic states. It is interesting to note that the base peak in the mass spectra induced upon irradiation of nitromethane at 228 nm with 10 ns laser pulses corresponds to NO^+, while the parent ion is not recorded. In contrast, upon irradiation with 50 fs pulses at 375 nm, the parent ion is the main feature in the mass spectra and the CH_3^+, NO_2^+, and NO^+ ions are also prominent.[17]

Wodtke *et al.*[9,18] confirmed experimentally that infrared multiphoton excitation of nitromethane could lead to CH_3O and NO fragments production *via* a nitro-to-nitrite rearrangement (NNR), resulting in the formation of CH_3ONO species (methylnitrite). Thus, the two main fragmentation pathways for neutral nitromethane are distinguished by a direct C–N bond rupture process:

$$CH_3NO_2 \rightarrow CH_3 + NO_2 \quad (1)$$

and a NNR pathway followed by NO loss:

$$CH_3ONO \rightarrow CH_3O + NO \quad (2)$$

These results were supported by the theoretical *ab initio* mapping of the rearrangement pathway performed by McKee,[19] who characterized the corresponding transition state and found that the NNR pathway is energetically competitive with the direct dissociation to NO_2. Bowman and Homayoon[20] have extended this picture through quasi-classical trajectory simulations, showing that NNR may occur through roaming-mediated isomerization. In this framework, initially proposed by Suits *et al.*[21] for the case of nitrobenzene, the NO_2 group separates but remains weakly bound to the methyl fragment as it roams before recombining to form CH_3ONO. This mechanism resembles the hydrogen-atom roaming dynamics originally proposed for formaldehyde by Townsend *et al.*[22] This type of process is often encountered in organic molecules. For instance, the H_2 roaming which leads to the formation of H_3^+ cation.[23,24] It should be noted, as pointed for the case of nitrobenzene by Giussani and Worth,[25] that roaming-accessible geometries bifurcate between NO_2 release and rearrangement, showing that roaming does not exclusively lead to NO loss, but can also lead to NO_2 elimination.

Department of Physics, University of Ioannina, 45110 Ioannina, Greece.
E-mail: kkosmid@uoi.gr

The rearrangement dynamics of neutral nitromethane have been studied by using ultrashort laser pulses and the timescales for NO_2 and methylnitrite formation have been reported ($\sim$85 and $\sim$450 fs, respectively) by applying fs pump (at 266 nm)/probe technique.[4]

Isomerization of nitromethane in the gas phase is not limited to the neutral molecule but is also possible in states of the parent ion.[26] Furthermore, it is reported that the initiation of the NNR is taking place in an electronically excited state (D_2) of nitromethane ion, and the process is completed within 500 fs, while OCH_3, which is clear evidence of NNR, is observed about 30 fs later.[10]

Thus, it is concluded that the cation could appear in three main isomeric structures: (a) nitromethane, (b) methylnitrite, formed through NNR, and (c) *aci*-nitromethane, generated *via aci*-isomerization, *i.e.* a hydrogen atom from the methyl group migrates and bonds to an oxygen atom, followed by the formation of a double bond between the carbon and nitrogen atoms. Therefore, the immediate question is whether isomerism is also possible in multiply charged ions whose production is feasible using strong laser fields. Recent theoretical and experimental studies on nitromethane in both solid state[27] and gas phase[28] have revealed the existence of additional structural isomers beyond methylnitrite and *aci*-nitromethane, including nitrosomethanol ($H_2C(NO)OH$) and the *N*-hydroxyoxaziridine (c-$CH_2NOH(O)$).

The interaction of nitromethane and nitroaromatic compounds with strong laser fields (10^{13}–10^{15} W cm^{-2}) in conjunction with mass spectrometry has been reported previously and the main feature was the observation of Coulomb explosion processes because of the generation of multiply charged parent molecules which subsequently fragment.[3,11,29]

More recently, Gutsev *et al.*[11] studied the interaction of nitromethane with intense laser beams (0.4–2.8 $\times$ 10^{14} W cm^{-2}) at λ = 1300 nm by recording the induced mass spectra. They concluded that the ejection of at least four electrons from the parent molecule is feasible under these irradiation conditions.

In the present work, we initially aim to determine the mechanism involved in the generation of multiply charged ions in the laser intensity range of $\sim 10^{14}$ W cm^{-2}, because it has not been elucidated systematically. A prerequisite for the investigation of the possible isomerization of the multiply charged parent ions is the correct identification of the different fragmentation channels. For this purpose, we studied the dependence of the fragment ions released on the phase of the asymmetric $\omega/2\omega$ fs laser field, which combined with the kinetic energies of the fragments allows the secure characterization of the dissociation routes. In a recent study,[30] it was observed that the production of H_2^+ and D_2^+ ionic fragments of water isotopologues depend on the laser wavelength. More specifically, an increase in the production of H_2^+ (and D_2^+ for heavy water) was attributed to the involvement of vibrational excitation. For this reason, the wavelength dependence of dissociative ionization of nitromethane is also explored. Finally, by studying the deuterated nitromethane (CD_3NO_2) under the same experimental conditions, we intended to gain insights about the isomerization and the dependence on laser field parameters.

Experimental

The experimental setup utilized has been described in detail previously.[30–32] The main parts of the setup are: (i) an optical parametric amplifier (OPA: Coherent, Opera Solo) pumped by 3 mJ pulses of $\sim$30 fs duration produced by a Ti:Sapphire laser system (Coherent, Legend Elite Duo USX) operating at λ_c = 800 nm, with 1 kHz repetition rate; (ii) an array of optics resulting in the synthesis of asymmetric $\omega/2\omega$ laser fields and allowing their phase control and (iii) a detection system (home-made Wiley–McLaren time-off-flight (ToF) mass spectrometer, where ions generated in the interaction region passing through a 0.1 cm diameter orifice are introduced into a 150 cm length field-free region).

Some additional details on the optical setup used to produce the asymmetric pulses are presented: to increase the diameter and eliminate the divergence of the OPA beam, two telescopes equipped with spherical silver mirrors are used. Then, the beam passes through a β-barium borate (BBO) crystal (600 μm thick) for second harmonic generation. The resulting ω and 2ω beams are guided co-linearly to a set of long-pass dichroic beam splitters (Thorlabs DMLP: with a cut on wavelength of 950 nm for the signal and 1180 nm for the idler beam), where they are separated and eventually recombined. The fundamental beam passes through a half-wave plate to rotate its polarization, aligning it with that of the 2ω beam and with the axis of the ToF-MS. In parallel, the 2ω beam is passing through a calcite ($CaCO_3$) plate (1.2 mm thick) mounted on an electronically controlled rotational stage with a step size $>0.01^\circ$ (with a temporal precision within hundreds of attoseconds[33]), introducing a controllable phase difference between the ω and 2ω beam. Hence, the investigation of ultrafast phenomena that depend on the shape of the field such as selective bond breaking and isomerization is possible.[34–36] The temporal overlapping of the two beams is achieved by utilizing a Mach–Zehnder-type interferometer. The shape of the asymmetric field also depends on the relative intensity of the two beams; thus, their intensity is independently controlled by using neutral density filters. The pulse duration for the OPA's signal beam is measured to be $\sim$40 fs (specifically for λ = 1150 and 1360 nm).

The beams are focused on the interaction region of the ToF-MS by a f = 5 cm spherical mirror. Circular polarization was achieved by using an achromatic quarter-waveplate.

The laser intensity at the interaction region is estimated by considering the beam characteristics (pulse energy, duration, size) and the focusing conditions. These intensity values are cross-checked by measuring the ratio of multiply charged Argon ions production (Ar^{2+}/Ar^+ and Ar^{3+}/Ar^{2+}) and compared to those reported previously.[37,38] We found a discrepancy of approximately 10% between these two intensity estimation approaches. The sample vapors are introduced effusively through a needle valve in the ToF spectrometer, and the working pressure is kept at approximately 5 $\times$ 10^{-7} mbar to avoid space charge effects.

The generated ions are accelerated by the two electric fields of the spectrometer (ΔV_1 = 500 V and ΔV_2 = 3000 V) and travel until they impinge on the detection system, which consists of two multichannel plates (MCPs) on a Chevron-type configuration.

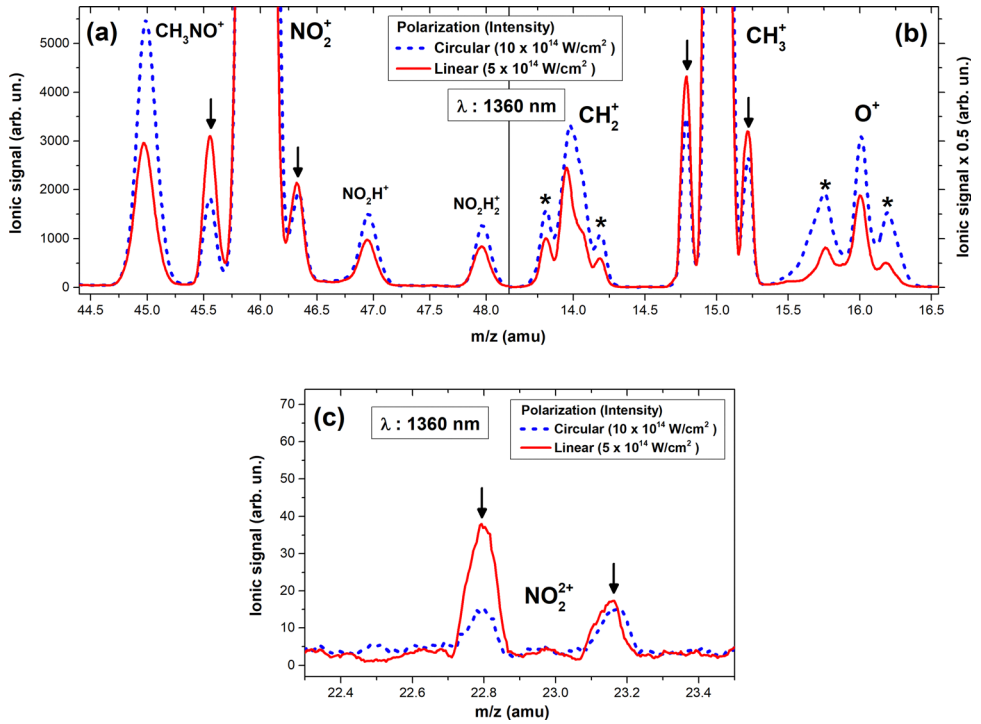

Fig. 1 Part of the ToF mass spectra of nitromethane recorded at 1360 nm for linear (red line) and circular (blue dashed line) polarized beams. The areas correspond to regions where (a) NO_2^+, (b) CH_3^+ and (c) NO_2^{2+} ionic fragments are recorded. The ionic signal axis for (a) graph is multiplied by the indicated factor on the (b) graph. The backward and forward components that correspond to ionic fragments released by the dissociation channels (3) and (5) are marked with black arrows.

The signal is preamplified and digitized using a multiple event digitizer (Fast-ComTech, P7888, quad 1 GHz time-of-flight/multi-scaler) with a storage resolution of 1 ns. For most of the $\omega/2\omega$ measurements, each spectrum was accumulated over 30 000 laser shots with an acquisition time of 30 s, whereas the single-beam mass spectra were recorded with 60 000 shots over 60 s.

The nitromethane (NM, $\geq$99.0%) and nitromethane-d3 (NM-d3, 99% atom D) samples used in the present work were purchased from Sigma-Aldrich.

Results and discussion

(i) Multiple ionization by single fs laser beams in IR region

The first question that needs to be answered concerns the process involved in the dissociative multiple ionization of nitromethane. The value of the Keldysh parameter γ[39] is a criterion often used to distinguish whether the multiple ionization is the result of multi-photon absorption (MPI) or tunneling processes facilitated by barrier suppression by the laser field. For values of γ much less than one, the ionization is considered to occur *via* the tunneling effect. In the present case, the value of the parameter γ ($\gamma = (I_p/2U_p)^{1/2}$), where I_p (= 11.07 eV[8]) is the ionization potential of nitromethane and U_p is the ponderomotive energy (U_p (eV) = 9.337 $\times$ 10^{-14} I (= 5 $\times$ 10^{14} W cm^{-2}) $\times$ λ^2 (= 1.36 μm) = 86.35 eV) is $\sim$0.25 $<$ 1.

Thus, this approach suggests that field-induced ionization (tunneling and/or above the threshold ionization) is more likely to be involved. It is noted, however, that multiple ionization of water was not attributed to tunneling ionization at similar laser intensities.[31]

To clarify the issue, we recorded the mass spectrum induced by a single beam at 1360 nm for linear and circular polarization. The pulse energy in the circularly polarized measurements was almost twice that of the linear one (thus $I_{circ} = 2 \times I_{lin}$), to irradiate the sample with beams having equal electric field amplitude.

Fig. 1 shows parts of the mass spectra recorded at 1360 nm with circular (blue dashed line) and linear (red line) polarization. As it is known, multiple ionization of molecules is usually accompanied by a Coulomb explosion, resulting in the ejection of ionic fragments towards the detector and in the opposite direction to it. The trajectory of the latter ions is reversed from the field in the interaction region, and they are detected with a time delay. This leads to the formation of complex-structured spectral features. By measuring the time difference between the forward and backward components and knowing the intensity of the accelerating field in the interaction region of the ToF-MS, it is possible to determine the kinetic energy of the released ionic fragments. In Fig. 1a is presented the part of the spectrum where the NO_2^+ ion (m/z = 46) is recorded. It is observed that apart from the backward and forward components of NO_2^+, all other peaks are recorded with greater abundance in the spectrum induced by the circularly polarized laser beam (the assignment as backward and forward components is supported by their dependence on the phase of $\omega/2\omega$ asymmetric laser field which will be discussed in the following section). Furthermore,

from Fig. 1c, the double-charged NO_2^{2+} (m/z = 23) ion is produced more efficiently when a linearly polarized beam is applied, even though the pulse energy is significantly reduced compared to that used in the circularly polarized experiments. These observations are conceivable in a framework of field-induced ionization, *i.e.* the suppression of the molecular potential barrier by the external laser field facilitates ionization *via* a tunneling process and the liberated electron returns towards the ionic core, when the phase of the field changes, and interacts with it, having gained ponderomotive energy. This rescattering process is sensitive to laser polarization since under circular polarization, it is probable that the returning electron misses the ionic core. Thus, we can conclude that the doubly (P^{2+}) and triply charged (P^{3+}) parent ions are generated *via* a rescattering process. Of course, the same dependence on laser polarization is also expected for the rest fragment ions released by the dissociation channel:

$$CH_3NO_2^{2+} \rightarrow CH_3^+ + NO_2^+. \quad (3)$$

Indeed, as depicted in Fig. 1b the same dependence on laser polarization is recorded for the backward and forward components of the CH_3^+ ion. Unfortunately, for the clear observation of the accompanying fragments of NO_2^{2+} from the dissociation of P^{3+} higher laser intensities needed to be applied but these laser intensities were impossible experimentally to be reached for the circularly polarized beam.

As mentioned above, the time separation between the backward and the forward components can be used to estimate the kinetic energy of the released fragment ions. Under the assumption that the Coulomb explosion takes place between two-point charges, the kinetic energy is calculated as:[40]

$$E_{kin}\,(eV) = 9.65 \times 10^{-7}\frac{(\Delta t)^2 z^2 F^2}{8m} \quad (4)$$

where Δt is the time difference (in ns) between the forward and backward components, z and m (in amu) are the charge and mass of the ionic fragment, and F (in V cm^{-1}) is the strength of the accelerating field. In cases where a neutral fragment is released, its kinetic energy is expected to be small compared to that from ejected ions *via* Coulomb explosion processes. Therefore, the influence on the estimated kinetic energy release (KER) for reactions involving Coulomb explosion is neglected in the present work. In order to reduce the error, the kinetic energies of the ionic fragments have been calculated for different F field strength values too. Thus, for the dissociation of the doubly charged parent ion (eqn (3)) the estimated kinetic energy values for CH_3^+ were found to be 3.6 ± 0.3 eV and for NO_2^+ equal to 1.2 ± 0.2 eV. These estimations result in a total kinetic energy released of KER = 4.8 ± 0.5 eV.

Fig. 2a shows spectra recorded at slightly higher intensity, to better depict the backward and forward peaks of CH_3^+ ions released as dissociation partners of NO_2^{2+} (the spectral features shown in Fig. 2a are marked with arrows). The correlation of these CH_3^+ peak components with those of NO_2^{2+} is verified based on momentum conservation and their dependence on the phase of the $\omega/2\omega$ asymmetric field, as will be discussed in following paragraphs. These ionic species are assigned to the dissociation of the triply charged parent ion *via* the channel:

$$CH_3NO_2^{3+} \rightarrow CH_3^+ + NO_2^{2+} \quad (5)$$

The kinetic energy of CH_3^+ calculated to be 6.3 ± 0.3 eV and for NO_2^{2+} equal to 2.2 ± 0.2 eV which leads to a KER = 8.5 ± 0.5 eV. As recently pointed out, these estimations are somewhat simplified because they do not consider the molecular binding energy, and the initial kinetic energy of the fragments accumulated from previous dissociation steps.[41] The latter is of importance for the case of the fragmentation in the triply charged parent case. Nevertheless, we can see that the calculated kinetic energy values are in excellent agreement with what is predicted by the conservation of momentum for both dissociation channels (eqn (3) and (5)).

Moreover, these KER values allow the estimation of the distance between the two fragments just before the Coulomb explosion *via* the equation:

$$KER\,(eV) = 14.4\frac{z_1 z_2}{r\,(Å)} \quad (6)$$

Therefore, for the case of two-body fragmentation in the dication, r is estimated to be 3.0 ± 0.3 Å, while for the triply

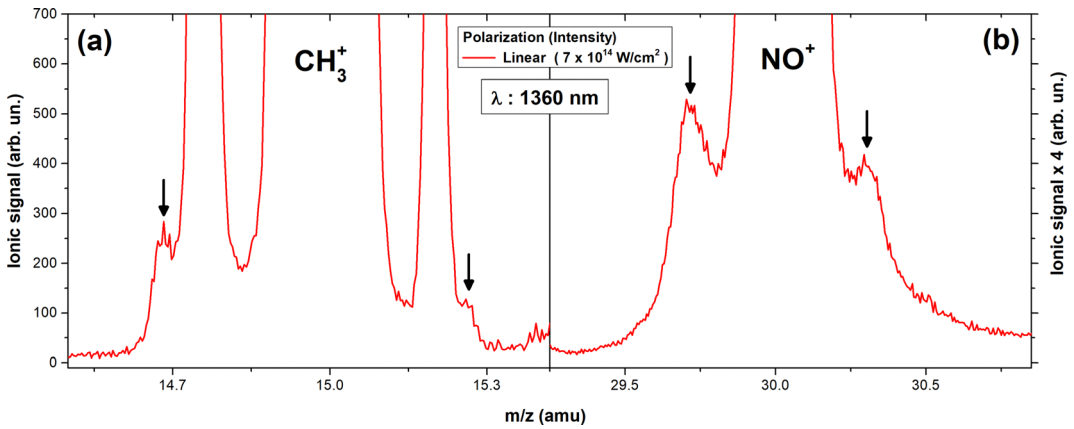

Fig. 2 Part of the ToF mass spectra of nitromethane recorded at 1360 nm for linear polarization. The areas correspond to regions where (a) CH_3^+ and (b) NO^+ ionic fragments are recorded. The backward and forward components that correspond to CH_3^+ released by the dissociation channel (5) and to NO^+ that originates from P^{3+} fragmentation are marked with black arrows.

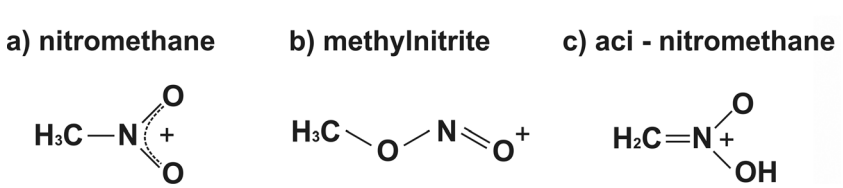

Scheme 1 A visual representation of the main isomeric structures of nitromethane cation.

charged parent, $r = 3.4 \pm 0.2$ Å. These values are longer than the C–N bond length in the ground state given to be $R_{eq} = 1.49$ Å.[42] The r value for the case of the triply charged parent ion is found to be slightly longer than that of the dication but within the experimental errors. The estimated KER and r values, which are different from those reported previously,[11] demonstrate extensive consistency with momentum conservation and the ionization mechanisms involved.

In Fig. 2b, the mass spectrum is shown magnified in the region of the NO^+ fragment and two low intensity side peaks (marked with black arrows) are observed. Assuming, at this stage, that these are forward and backward components of NO^+ released *via* a Coulomb explosion process, their kinetic energy is estimated to be 1.5 ± 0.2 eV. The origin of these NO^+ ions will be discussed in the following paragraph.

(ii) Multiple ionization by $\omega/2\omega$ fs asymmetric laser fields

In the previous paragraphs, we referred to the mechanism of multiple ionization of nitromethane while the molecule maintains the original structure. However, the appearance in the mass spectra of ions with $m/z = 30$ (NO^+) or $m/z = 31$ (CH_3O^+ or HNO^+) is understandable by considering these as fragments following a molecular rearrangement process induced by the electromagnetic field. The rearrangement processes that lead to isomeric forms of nitromethane have been studied extensively in the past.[9,18,19,26,43–46] At least three forms are mentioned in the literature that are presented in Scheme 1 for the nitromethane cation.

The mechanisms that lead to these isomeric forms have been investigated extensively, while the dynamics of these processes have been studied experimentally too.[4,10] In recent years, the isomerism of nitromethane has been interpreted in the context of a roaming process characterized by a loose transition state resulting in methylnitrite structure. Nevertheless, many issues involved in molecular isomerization remain unclear. Thus, we performed experiments utilizing $\omega/2\omega$ fs asymmetric laser fields to gain more insight into these processes.

In Fig. 3 (top) the mass spectra induced by a $\lambda_{\omega/2\omega}$: 1360/680 nm at (a) $I = 4.5 \times 10^{14}$ W cm^{-2} and (b) $I = 1.5 \times 10^{15}$ W cm^{-2} (at $\Delta\phi = \pi$) $\omega/2\omega$ asymmetric field is depicted. Moreover, parts of the spectra corresponding to the region of NO_2^+, CH_3^+ and NO_2^{2+} recorded for two different phases of the asymmetric laser field ($\Delta\phi = \pi$ and $\Delta\phi = 0$) are presented expanded in Fig. 3c, d and e respectively. A zero-phase difference ($\Delta\phi = 0$) between the ω and 2ω fields is defined as the case that results in an asymmetric field having its maximum intensity towards the repeller, while $\Delta\phi = \pi$ indicates that the maximum intensity is pointed towards the MCP detector. The phase of the asymmetric field was determined by recording simultaneously the mass spectra of nitromethane and that of carbon monoxide (CO) which was analyzed in previous works.[47] Another experimental parameter that is important to be controlled is the electric field strength ratio $\left(\gamma = \frac{E_{2\omega}}{E_\omega} = \sqrt{\frac{I_{2\omega}}{I_\omega}}\right)$ of the participating beams ($\omega/2\omega$) in the composition of the asymmetric field.

We have performed experiments with different γ values. It was confirmed that for the reliable identification of the dissociation channels the best value is $\gamma \sim 0.6$.[32] Thus, the value of γ for the asymmetric laser field has been chosen after checking the variation of the amplitude of β parameter as a function of intensity ratio $I_{2\omega}/I_\omega$ similarly to that described in previous work.[32]

Similar spectra have been also recorded for $\lambda_{\omega/2\omega}$: 1150/575 nm, 1250/625 nm, 1700/850 nm and 1800/900 nm and for laser intensities in the region of 4×10^{14} to 1.5×10^{15} W cm^{-2}.

From Fig. 3c–e it is obvious that the backward and forward components depend on the phase of the asymmetric field. These peak components are attributed to ions ejected by Coulomb explosion processes within multiply charged parent ions, and their abundance varies with the phase of the asymmetric $\omega/2\omega$ field.

Fig. 4a and b show the dependence of various ionic fragments on the phase of $\omega/2\omega$ laser field for $\lambda_{\omega/2\omega}$: 1150/575 nm, at $I = 5 \times 10^{14}$ W cm^{-2} and $I = 10 \times 10^{14}$ W cm^{-2} respectively. The ordinate of the 4a and b represents the asymmetry parameter β defined by the relation:

$$\beta = \frac{Y_{forw} - Y_{back}}{Y_{forw} + Y_{back}} \quad (7)$$

where Y_{forw} and Y_{back} refer to the total area yield of the forward and backward component of the specific ionic species.

First, regarding the dissociation channels (for dication reaction (3) and for trication reaction (5), as discussed previously) that take place while the molecule maintains its nitromethane structure (Scheme 1a), we observe that indeed the fragments NO_2^+ (1.2 eV) and CH_3^+ (3.6 eV) are ejected from the dication in opposite directions (their β maxima exhibit $\Delta\phi = \pi$). The same phase difference is observed for NO_2^{2+} (2.2 eV) and CH_3^+ (6.3 eV). Therefore, considering also the conservation of momentum presented above, there is no doubt that eqn (3) and (5) represent the two-body fragmentation channels from nitromethane dication and trication isomers.

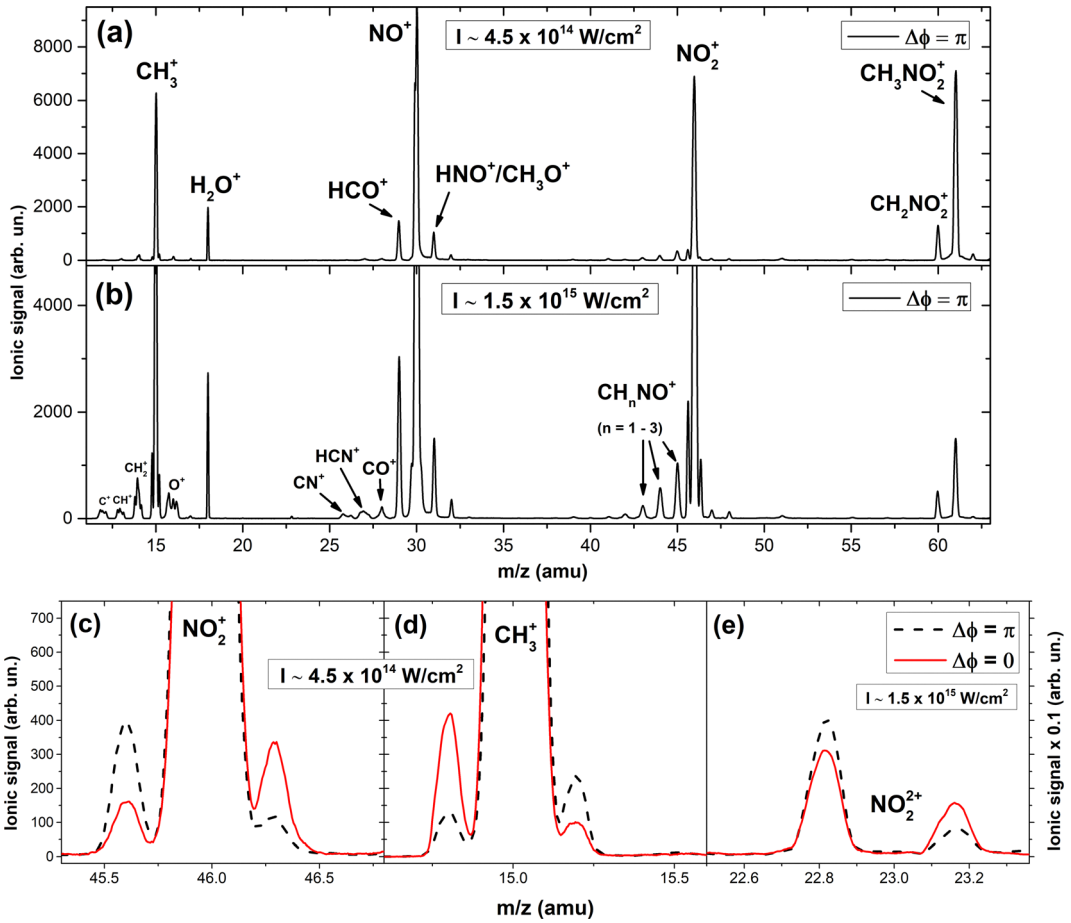

Fig. 3 Top: The ToF mass spectra induced by an asymmetric phase controlled $\omega/2\omega$ laser field of $\lambda_{\omega/2\omega}$: 1360/680 nm at $\Delta\varphi = \pi$, (a) $I = 4.5 \times 10^{14}$ W cm^{-2} and (b) $I = 1.5 \times 10^{15}$ W cm^{-2}. Bottom: The areas corresponding to (c) NO_2^+, (d) CH_3^+ (for $I = 4.5 \times 10^{14}$ W cm^{-2}) and (e) NO_2^{2+} (for $I = 1.5 \times 10^{15}$ W cm^{-2}) are depicted. The black dashed line corresponds to $\Delta\phi = \pi$ and the red line to $\Delta\phi = 0$. The electric field strengths ratio (γ) of the participating beams ($\omega/2\omega$) was $\gamma \sim 0.6$. The ionic signal axes for (c) and (d) graphs are the same and for (e) multiplied by the indicated factor.

Second, between the NO_2^+, NO_2^{2+}, NO^+ and O^+ ions there is no phase difference, *i.e.* they are ejected in the same direction from the parent ions which confirms that NO^+ (1.5 eV) ions are not products of NO_2^{n+} (n = 2, 3) dissociation and their appearance in the mass spectra is related to molecular isomerization. This isomerization has been studied extensively, and it is described by the following process:

$$CH_3NO_2^+ \rightarrow CH_3ONO^+ \rightarrow NO^+ + CH_3O \quad (8)$$

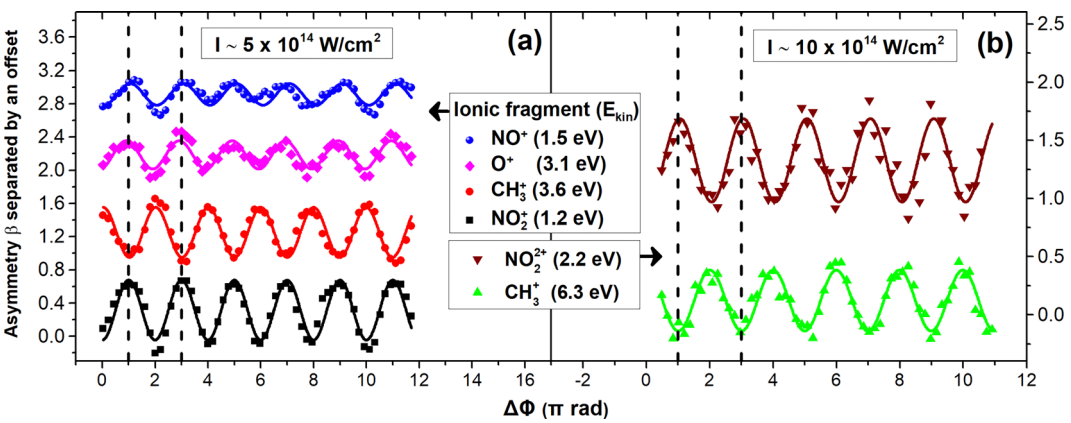

Fig. 4 Asymmetry parameter (β) measurements of the ionic fragments (NO_2^+, NO_2^{2+}, CH_3^+, NO^+ and O^+) recorded for $\lambda_{\omega/2\omega}$: 1150/575 nm, at (a) $I = 5 \times 10^{14}$ W cm^{-2} and (b) $I = 10 \times 10^{14}$ W cm^{-2}. The vertical dashed line and the sinusoidal fit are used for eye guiding purposes.

It has been determined that after C–N bond rupture, the NO_2 moiety is rotating in proximity, for about 500 fs. While NO_2 rotates, an oxygen atom reaches the CH_3 radical resulting in a C–O bond formation and molecular isomerization (methylnitrite). NO^+ is released from the new molecular structure after ~30 fs.[10]

Obviously, the NO^+ (1.5 eV) side peaks depicted in Fig. 2b are not released *via* eqn (8). Their dependence on the phase of the $\omega/2\omega$ laser field (Fig. 4a) indicates that these are backward and forward components formed after a Coulomb explosion process occurring on a multiply charged parent ion. However, two-body fragmentation in the dication is not supported by the present data because the expected accompanying fragment ion (m/z = 31) is recorded with a single peak profile (Fig. 3a and b). Furthermore, a three-body fragmentation process of the methylnitrite dication that results in NO^+, with two (CH_3 and O) accompanying fragments of which one is singly charged, is excluded. Specifically, the case of charged methyl fragments (CH_3^+, E_{kin} = 3.6 eV) is ruled out as they are defined as dissociation partners of NO_2^+ (1.2 eV) based on their abundance, dependence on laser polarization and momentum conservation, while the case of O^+ as an accompanying fragment ion is also rejected because there is no phase difference in the maxima of the β asymmetry parameter between NO^+ and O^+ ions ($\Delta\phi$ = 0). Thus, these NO^+ ions are expected to be generated in triply charged parent ions in agreement with that proposed earlier.[11] From this point of view, it seems that the fragmentation of dication to NO_2^+ is more probable compared to that into NO^+ ions. This conclusion does not imply that isomerization is not probable to proceed in the dication.

On the other hand, isomerization in cation is manifested also by the presence of single peak ions at m/z = 31 in the mass spectra. Such ions could be assigned to CH_3O^+ and/or HNO^+. The generation of these two fragments is preceded by a molecular rearrangement like the following:

$$CH_3NO_2^+ \rightarrow CH_3ONO^+ \rightarrow CH_3O^+ + NO \quad (9)$$

$$\rightarrow HNO^+ + CH_2O \quad (10)$$

In addition, two other spectral features shown in Fig. 1a indicate molecular isomerism. We refer to ions with m/z = 47 and m/z = 48. Their single-peak profiles suggest that they are liberated from the single charged parent ion. The ion m/z = 47 has been assigned as $HONO^+$ and is a fragment generated after isomerization to methylnitrite.[3,27] The peak at m/z = 48 is arising from the loss of –CH from the parent ion. It should be noted that in the mass spectra of deuterated nitromethane, the corresponding peak (m/z = 50) is extremely weak. Thus, although it is certain that this ion is produced in an isomerized structure, its origin cannot be determined based on the present data.

(iii) Gaining insight from deuterated nitromethane

As it appears from the reactions described by eqn (9) and (10), it is impossible to assign the ions recorded at m/z = 31 and consequently the contribution of these dissociation channels. This difficulty is circumvented by performing the same experiments for deuterated nitromethane because the ions released from channel (9) are expected to be observed at m/z = 34 (CD_3O^+) while those from channel (10) at m/z = 32 (DNO^+).

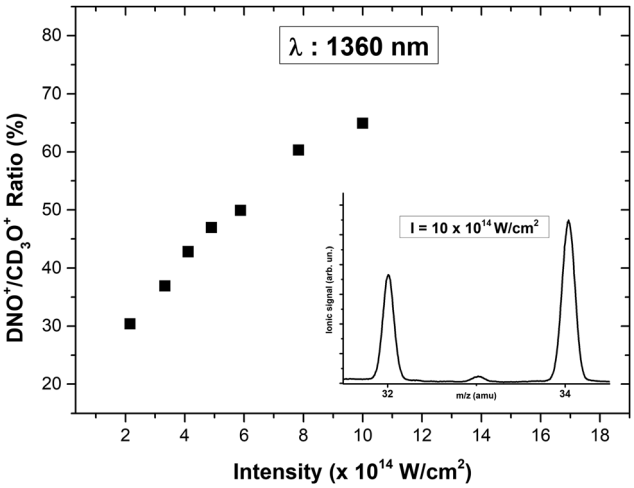

Fig. 5 Dependence of ionic fragments DNO^+/CD_3O^+ abundance ratio on the laser intensity at 1360 nm for the deuterated nitromethane. In the insert, the magnified mass spectrum region is depicted (λ = 1360 nm, I = 10×10^{14} W cm^{-2}) where peaks at m/z = 32 (DNO^+) and m/z = 34 (CD_3O^+) are detected. The small peak at (m/z = 33) assigned as CD_2HO^+ is arising from a –NO loss channel of the $CD_2HNO_2^+$ which is present as an impurity in the sample.

In the insert of Fig. 5 the mass spectrum of deuterated nitromethane at 1360 nm is presented magnified where single peaks at m/z = 32 and m/z = 34 have been recorded.

To gain a better understanding, the dependence of the abundance ratio of these two ions on the laser intensity was investigated. We found that the value of the DNO^+/CD_3O^+ abundance ratio increases with increasing laser intensity (Fig. 5). At first sight, this could suggest that the abundance of DNO^+ increases because the D-migration to the NO side of the isomerized molecular ion is facilitated by the effective suppression of potential barriers by the increased laser field intensity. However, since the production of DNO^+ follows the isomerization,[20,43] which is completed on a time scale much longer than the pulse duration of the laser used, this approach should be considered as not very likely. On the other hand, the ratio could increase because the denominator decreases, *i.e.*, due to the depletion of CD_3O^+ as the laser intensity increases. The depletion of CD_3O^+ could be understood by the reasonable assumption that as the laser intensity increases, involvement of higher excited molecular states is expected and the CD_3O^+ could be released in an excited state that leads to a further fragmentation by a –D loss. Thus, while the CD_3O^+ is depleted, the spectral feature at m/z = 32 gains intensity since there is a contribution from both DNO^+ and CD_2O^+. In this approach the dependence on the laser intensity of the abundance ratio presented in Fig. 5 is conceivable.

(iv) Investigation of the dependence on the intensity and the wavelength of the $\omega/2\omega$ fields

Having observed the variation of the ion's abundance ratio as a function on laser intensity (Fig. 5), the following step was to

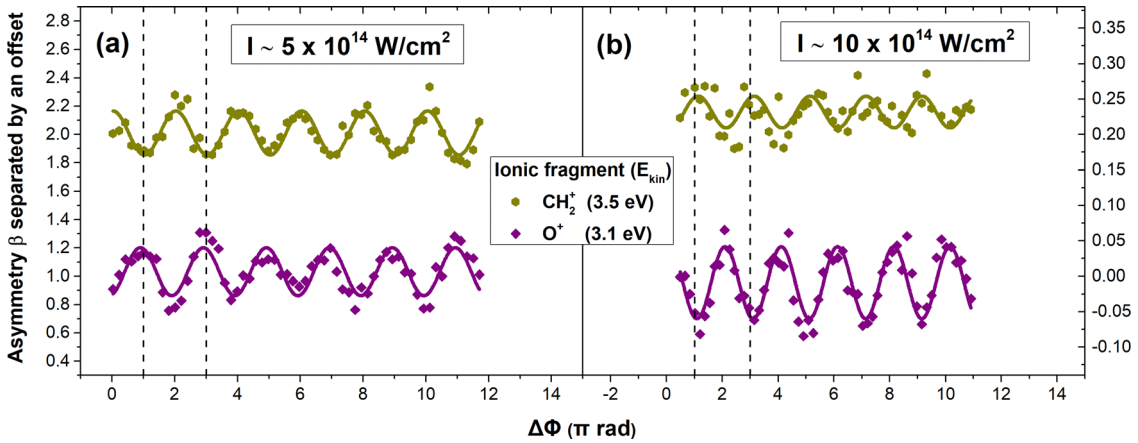

Fig. 6 Asymmetry parameter (β) measurements of the ionic fragments CH_2^+ (3.5 eV) and O^+ (3.1 eV) recorded for $\lambda_{\omega/2\omega}$: 1150/575 nm, at (a) $I = 5 \times 10^{14}$ W cm^{-2} and (b) $I = 10 \times 10^{14}$ W cm^{-2}. The vertical dashed line and the sinusoidal fit are used for eye guiding purposes.

explore if there is any dependence on the intensity of the $\omega/2\omega$ fields. In this case, interest is focused on the dependence of the ionic fragments of nitromethane on the phase of the asymmetric field as its intensity varies. All measurements were performed by keeping the same intensity ratio $\gamma \sim 0.6$ for the $\omega/2\omega$ fields while the phase calibration was achieved by a simultaneous presence of CO in the interaction region.

We investigated the dependence of the β parameter for all ionic species on the laser field intensity. We found that for intensity values greater than $\geq 8 \times 10^{14}$ W cm^{-2} a striking change occurs in the β parameter maxima of components constituting the CH_2^+ and O^+ peaks: a phase jump by π *i.e.* the position of their maxima is reversed. This change is observed only for these two fragment ions.

In Fig. 6 the asymmetry parameter β for CH_2^+ and O^+ with respect to the phase of the asymmetric field is presented (the vertical dashed lines indicate the $\Delta\phi$ values where the β parameter maxima are recorded for NO_2^+).

In Fig. 6 the change of the asymmetry parameter of these two ions observed at two laser field intensities is depicted while for the intermediate range of intensities (6–8 $\times 10^{14}$ W cm^{-2}) it was not possible to record a clear sinusoidal change in the β parameter as a function of the phase of the asymmetric field.

Seeking the origin of these two fragments firstly it should be noted that the different dependence on laser polarization of the back- and forward components of CH_3^+ compared to the CH_2^+ ions (Fig. 1b, CH_2^+ and O^+ backward and forward peaks are marked with stars) indicate that these fragments are produced by a different dissociation pathway. Secondly, the phase difference ($\Delta\phi = \pi$) for β parameter maxima for CH_2^+ and O^+ ions implies that these ions are ejected in opposite directions, and this observation is valid even when the positions of maxima are changed. The fact that it occurs simultaneously and only for CH_2^+ and O^+ indicates that they have a common precursor. Such a precursor should be a doubly charged ion, and it could be the product of a charged asymmetric fragmentation:

$$P^{2+} \rightarrow CH_2O^{2+} + HNO \qquad (11)$$

The involvement of higher charged parent ions is excluded because the HNO^+ ions are recorded always as single peak. Alternatively, the dication could initially fragment to CH_3O^{2+} which subsequently dissociates by H-loss. It is of significance to note that in the mass spectra of nitromethane a tiny peak at $m/z = 15.5$ corresponding to CH_3O^{2+} is observed and that these processes are taking place in isomerized molecules.

The generated CH_2O^{2+} ions fragment following the reaction:

$$CH_2O^{2+} \rightarrow CH_2^+ + O^+ \qquad (12)$$

The validity of eqn (12) can be checked by the estimated kinetic energies of the released ions. The kinetic energies of CH_2^+ and O^+ found to be 3.5 $\pm$ 0.3 eV and 3.1 $\pm$ 0.3 eV respectively and these values satisfy the momentum conservation principle for the reaction described in eqn (12).

As far as the change in the positions of the β parameter maxima of CH_2^+ and O^+ ions is concerned, it reflects the orientation dependence of the dissociative ionization probability, which is mainly determined by the shape of the molecular orbital.

The change may be due to the contribution to the molecular double ionization of an electron from a different molecular orbital. The three highest occupied molecular orbitals $\ldots\ldots(5a'')^2(10a')^2(6a'')^2$ (assuming that the molecule belongs to the C_s symmetry group).[8]

The ionization potential values of these orbitals are very close and have been experimentally determined to be 11.08, 11.73 and 11.95 eV respectively.[8] However, the charge distribution they represent are drastically different, while HOMO [n_π(O)] excitation involves lone-pair electrons located on atomic oxygen, in HOMO−1 [(σ(CN) + π(NO_2)] case the electronic cloud is widely distributed in the molecular skeleton. Therefore, increasing the laser power can induce excitation from HOMO−1, that eventually is imprinted as a change in the positions of the β-parameter maxima.

It is interesting to mention that in the context of the interpretation of experimental data concerning the molecular interaction with strong laser fields, a multielectron polarization (MEP) term has been included in the theoretical description,

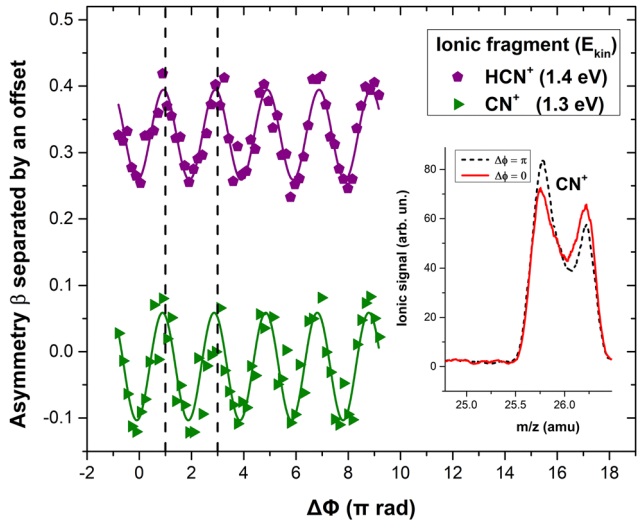

Fig. 7 Asymmetry parameter (β) measurements of ionic fragments CN^+ (1.3 eV) and HCN^+ (1.4 eV) recorded at $\lambda_{\omega/2\omega}$: 1360/680 nm and $I = 1.5 \times 10^{15}$ W cm^{-2}. The vertical dashed line and the sinusoidal fit are used for eye guiding purposes. In the insert the magnified mass spectrum region is presented where the ionic fragment CN^+ at m/z = 26 is observed. The black dashed line corresponds to $\Delta\phi = \pi$ and the red line to $\Delta\phi = 0$.

i.e. an induced dipole term that describes the interaction of the outgoing electron with the ionic core.[48] In this framework, Abu-samha and Madsen[49] have explained the orientation-dependent total ionization yield for oriented OSC molecules. In addition, their theoretical calculations show that while the orientation angle of the maximum total ionization yield is independent of the laser intensity, the contribution from the degenerate HOMOs of the OCS molecule varies as the laser intensity increases. So, there is a notable resemblance between the theoretical predictions above and those we record experimentally for nitromethane. Indeed, it appears that the contribution to ionization from different molecular orbitals could be captured in measurements of the asymmetry parameter β.

As said in the introduction, one aim of the present work was the investigation of the dependence of the dissociation of nitromethane on laser wavelength. Indeed, we performed experiments with single beam (λ = 1150, 1250, 1300, 1360, 1700, 1800 nm) without observing any change of the dissociation pattern of nitromethane. Moreover, no change of the maxima of the asymmetric parameter β position (phase shifts) observed as the composition of the $\omega/2\omega$ was varied ($\lambda_{\omega/2\omega}$ = 1150/575, 1250/625, 1360/680, 1700/850, 1800/900 nm).

In the analysis up to this point, the possibility of isomerization to *aci*-nitromethane, *N*-hydroxyoxaziridine and nitrosomethanol has not been discussed. However, it is important to note that at higher laser intensities applied ($\geq 10^{15}$ W cm^{-2}) backward and forward peaks at m/z = 26 and 27 have been recorded. These peaks are unambiguously assigned to CN^+ and HCN^+ ions. The part of the mass spectrum for m/z = 26 is shown as an insert in Fig. 7. Similarly, in the spectrum of the deuterated isotopologue, at the same laser intensities, peaks at m/z = 26 and m/z = 28 (DCN^+) have been also observed. The origin of these peaks should be the *aci*-nitromethane isomer because, as depicted in Scheme 1c, only in this isomer there is a double bond between carbon and nitrogen atoms, which means that C=N bond cleavage could be achieved under even stronger laser irradiation.

The kinetic energies of these fragments are calculated to be 1.3 ± 0.2 eV for CN and 1.4 ± 0.2 eV for HCN (DCN) (for both isotopologues). Regarding their dependence on the phase of the $\omega/2\omega$ field, the maxima and minima of the β parameter (Fig. 7) are observed at the same phase positions as those of NO_2^+. Our assessment is that these ions are products of at least three body fragmentation processes. The present experimental data does not provide the basis for drawing further safe conclusions regarding isomerization to *aci*-nitromethane. Thus, the discussion is mainly limited to establishing the existence of this isomer under the conditions of the present experiment.

To summarize the proposed fragmentation pathways and assigned isomers for the main diagnostic fragments discussed in this work we present the following table (Table 1).

Conclusions

In this work, it was initially demonstrated that dissociative multiple ionization of nitromethane can be achieved through a

Table 1 The main ionic fragments discussed in this work with their calculated kinetic energies, phase dependence, assigned isomer, fragmentation pathway and the associated figure(s)

m/z (amu)	Assigned fragment[a]	Kinetic energy ± error[b] (eV)	Phase difference[c]	Assigned isomer	Associated figure(s)	Fragmentation pathway
46	NO_2^+	1.2 ± 0.2	0	Nitromethane	Fig. 1a, 3c and 4a	(3)
15	CH_3^+	3.6 ± 0.3	π	Nitromethane	Fig. 1b, 3d and 4a	(3)
15	CH_3^+	6.3 ± 0.3	π	Nitromethane	Fig. 2a and 4b	(5)
23	NO_2^{2+}	2.2 ± 0.2	0	Nitromethane	Fig. 1c, 3e and 4b	(5)
30	NO^+	1.5 ± 0.2	0	Methylnitrite	Fig. 2b and 4a	—
16	O^+	3.1 ± 0.3	0 π^d	Methylnitrite	Fig. 1b, 4a and 6	(12)
14	CH_2^+	3.5 ± 0.3	π 0^d	Methylnitrite	Fig. 1b and 6	(12)
26	CN^+	1.3 ± 0.2	0	*aci*-Nitromethane	Fig. 7	—
27	HCN^+	1.4 ± 0.2	0	*aci*-Nitromethane	Fig. 7	—

[a] Assigned fragment based on the current study and the available literature. [b] Calculated kinetic energy values for the corresponding ionic fragments with the appropriate experimental error values. [c] Phase difference of the asymmetry parameter β of each fragment ion with respect to that of O^+ ejected from the CO_2^+ dissociation (phase calibration). [d] The left-side value of the phase difference corresponds to the data recorded at $I = 5 \times 10^{14}$ W cm^{-2} while the right-side value to that at $I = 10 \times 10^{14}$ W cm^{-2}.

rescattering process. It was found that the dications and the triply charged parent ions of nitromethane generated by rescattering can be fragmented by a direct C–N bond cleavage. The kinetic energies of the ionic fragments have been calculated and in conjunction with data acquired from experiments utilizing $\omega/2\omega$ asymmetric fs laser fields, the main dissociation channels were determined with certainty.

The presence in the mass spectra of at least three possible isomeric structures has been verified.

Isomerization to methylnitrite is more likely in singly charged parent ion. The dissociation follows a roaming process which is completed in a longer time than the duration of the laser pulse used. The rotation of the NO_2 moiety facilitates the methylnitrite formation which fragments to release NO^+, $HONO^+$, H_2ONO^+ at low laser intensities. The presence of the *aci*-nitromethane isomer is characterized by the observation of HCN^+ and CN^+ ionic fragments at high field intensities.

Examining the laser intensity dependence of fragmentation reveals in the case of deuterated isotopologues that the abundance ratio of DNO^+ and CD_3O^+ varies as a function of laser intensity. This dependence is attributed to a –D loss process from CD_3O^+.

Furthermore, based first on the observation that only for CH_2^+ and O^+ ions the asymmetry parameter β maxima exhibits a drastic shift as the $\omega/2\omega$ field intensity increases, and second on the calculated kinetic energies of these two ions, it is concluded that it is more likely that these ions have a common precursor assigned to CH_2O^{2+}. The latter is proposed to be generated *via* an asymmetric charged dissociation channel of the methylnitrite dication. The possibility of the existence of such a channel is discussed for the first time.

The above observations are attributed to the contribution to ionization from HOMO−1 and the change that this entails in the orientation dependence of the dissociative ionization probability. This change is imprinted on the asymmetry parameter β maxima shifts.

Therefore, additional possibilities are emerging offered by utilizing asymmetric $\omega/2\omega$ fs laser fields for the study of molecular processes.

Author contributions

P. Vamvakidis: data curation, formal analysis investigation, methodology, writing – original draft, C. Kosmidis: conceptualization, data curation, investigation, methodology, resources, supervision, writing – original draft.

Conflicts of interest

There are no conflicts to declare.

Data availability

Data will be made available on request.

Acknowledgements

The experiments were performed in the Central Laser Facility of the University of Ioannina, and we would like to express our thanks for the use of their facilities.

References

1 A. D. Tasker, L. Robson, K. W. D. Ledingham, T. McCanny, S. M. Hankin, P. McKenna, C. Kosmidis, D. A. Jaroszynski and D. R. Jones, *J. Phys. Chem. A*, 2002, **106**, 4005–4013.
2 C. Kosmidis, A. Marshall, A. Clark, R. M. Deas, K. W. D. Ledingham and R. P. Singhal, *Rapid Commun. Mass Spectrom.*, 1994, **8**, 607–614.
3 H. S. Kilic, K. W. D. Ledingham, C. Kosmidis, T. McCanny, R. P. Singhal, S. L. Wang, D. J. Smith, A. J. Langley and W. Shaikh, *J. Phys. Chem. A*, 1997, **101**, 817–823.
4 T. Nelson, J. Bjorgaard, M. Greenfield, C. Bolme, K. Brown, S. McGrane, R. J. Scharff and S. Tretiak, *J. Phys. Chem. A*, 2016, **120**, 519–526.
5 K. P. Shrestha, N. Vin, O. Herbinet, L. Seidel, F. Battin-Leclerc, T. Zeuch and F. Mauss, *Fuel*, 2020, **261**, 116349.
6 L. V. S. Dalagnol, M. H. F. Bettega, N. C. Jones, S. V. Hoffmann, A. Souza Barbosa and P. Limão-Vieira, *J. Phys. Chem. A*, 2023, **127**, 1445–1457.
7 Y. Q. Guo, A. Bhattacharya and E. R. Bernstein, *J. Phys. Chem. A*, 2009, **113**, 85–96.
8 A. Shastri, A. K. Das, K. Sunanda and B. N. Rajasekhar, *J. Quant. Spectrosc. Radiat. Transfer*, 2021, **276**, 107933.
9 A. M. Wodtke, E. J. Hintsa and Y. T. Lee, *J. Chem. Phys.*, 1986, **84**, 1044–1045.
10 M. D. Word, H. A. López Peña, D. Ampadu Boateng, S. L. McPherson, G. L. Gutsev, L. G. Gutsev, K. U. Lao and K. M. Tibbetts, *J. Phys. Chem. A*, 2022, **126**, 879–888.
11 G. L. Gutsev, S. L. McPherson, H. A. López Peña, D. A. Boateng, L. G. Gutsev, B. R. Ramachandran and K. M. Tibbetts, *J. Phys. Chem. A*, 2020, **124**, 7427–7438.
12 M. Sumida, Y. Kohge, K. Yamasaki and H. Kohguchi, *J. Chem. Phys.*, 2016, **144**, 064304.
13 D. B. Moss, K. A. Trentelman and P. L. Houston, *J. Chem. Phys.*, 1992, **96**, 237–247.
14 S. Adachi, H. Kohguchi and T. Suzuki, *J. Phys. Chem. Lett.*, 2018, **9**, 270–273.
15 A. Dey, R. Fernando, C. Abeysekera, Z. Homayoon, J. M. Bowman and A. G. Suits, *J. Chem. Phys.*, 2014, **140**, 054305.
16 L. J. Butler, D. Krajnovich, Y. T. Lee, G. Ondrey and R. Bersohn, *J. Chem. Phys.*, 1983, **79**, 1708–1722.
17 K. W. D. Ledingham, R. M. Deas, A. Marshall, T. McCanny, R. P. Singhal, H. S. Kilic, C. Kosmidis, A. J. Langley and W. Shaikh, *Rapid Commun. Mass Spectrom.*, 1995, **9**, 1522–1527.
18 A. M. Wodtke, E. J. Hintsa and Y. T. Lee, *J. Phys. Chem.*, 1986, **90**, 3549–3558.
19 M. L. McKee, *J. Phys. Chem.*, 1989, **93**, 7365–7369.

20 Z. Homayoon and J. M. Bowman, *J. Phys. Chem. A*, 2013, **117**, 11665–11672.
21 M. L. Hause, N. Herath, R. Zhu, M. C. Lin and A. G. Suits, *Nat. Chem.*, 2011, **3**, 932–937.
22 D. Townsend, S. A. Lahankar, S. K. Lee, S. D. Chambreau, A. G. Suits, X. Zhang, J. Rheinecker, L. B. Harding and J. M. Bowman, *Science*, 2004, **306**, 1158–1161.
23 N. Ekanayake, T. Severt, M. Nairat, N. P. Weingartz, B. M. Farris, B. Kaderiya, P. Feizollah, B. Jochim, F. Ziaee, K. Borne, K. Raju P., K. D. Carnes, D. Rolles, A. Rudenko, B. G. Levine, J. E. Jackson, I. Ben-Itzhak and M. Dantus, *Nat. Commun.*, 2018, **9**, 5186.
24 S. Kwon, S. Sandhu, M. Shaik, J. Stamm, J. Sandhu, R. Das, C. V. Hetherington, B. G. Levine and M. Dantus, *J. Phys. Chem. A*, 2023, **127**, 8633–8638.
25 A. Giussani and G. A. Worth, *J. Phys. Chem. Lett.*, 2024, **15**, 2216–2221.
26 H. Egsgaard, L. Carbea and S. Elbel, *Ber. Bunsen-Ges. Phys. Chem.*, 1986, **90**, 369–374.
27 S. K. Singh and R. I. Kaiser, *Chem. Phys. Lett.*, 2021, **766**, 138343.
28 S. K. Singh, T. Y. Tsai, B. J. Sun, A. H. H. Chang, A. M. Mebel and R. I. Kaiser, *J. Phys. Chem. Lett.*, 2020, **11**, 5383–5389.
29 C. Kosmidis, K. W. D. Ledingham, H. S. Kilic, T. McCanny, R. P. Singhal, A. J. Langley and W. Shaikh, *J. Phys. Chem. A*, 1997, **101**, 2264–2270.
30 E. Kechaoglou and C. Kosmidis, *Chem. Phys. Lett.*, 2020, **756**, 137835.
31 E. Kechaoglou and C. Kosmidis, *Int. J. Mass Spectrom.*, 2023, **483**, 116967.
32 E. Kechaoglou, K. Ferentinou, S. Kaziannis and C. Kosmidis, *J. Chem. Phys.*, 2021, **154**, 244306.
33 H. Ohmura, N. Saito and T. Morishita, *Phys. Rev. A: At., Mol., Opt. Phys.*, 2011, **83**, 063407.
34 T. Endo, H. Fujise, Y. Kawachi, A. Ishihara, A. Matsuda, M. Fushitani, H. Kono and A. Hishikawa, *Phys. Chem. Chem. Phys.*, 2017, **19**, 3550–3556.
35 H. Ohmura and T. Nakanaga, *J. Chem. Phys.*, 2004, **120**, 5176–5180.
36 H. Ohmura, T. Nakanaga and M. Tachiya, *Phys. Rev. Lett.*, 2004, **92**, 113002.
37 E. F. Sistrunk, PhD thesis, The Ohio State University, 2011.
38 S. Larochelle, A. Talebpour and S. L. Chin, *J. Phys. B: At., Mol. Opt. Phys.*, 1998, **31**, 1201–1214.
39 L. V. Keldysh, *J. Exp. Theor. Phys.*, 1965, **20**, 1945–1957.
40 W. C. Wiley and I. H. McLaren, *Rev. Sci. Instrum.*, 1955, **26**, 1150–1157.
41 W. Jiang, X. Wang, S. Zhang, R. Dong, Y. Guo, J. Feng, Z. Shen, T. Yan, Z. Zhu and Y. Jiang, *J. Chem. Phys.*, 2022, **157**, 084302.
42 A. P. Cox and S. Waring, *J. Chem. Soc., Faraday Trans. 2*, 1972, **68**, 1060–1071.
43 M. Isegawa, F. Liu, S. Maeda and K. Morokuma, *J. Chem. Phys.*, 2014, **140**, 244310.
44 R. P. Saxon and M. Yoshimine, *Can. J. Chem.*, 1992, **70**, 572–579.
45 M. L. Mckee, *J. Phys. Chem.*, 1986, **90**, 2335–2340.
46 C. Lifshitz, M. Rejwan, I. Levin and T. Peres, *Int. J. Mass Spectrom. Ion Processes*, 1988, **84**, 271–282.
47 E. Kechaoglou, S. Kaziannis and C. Kosmidis, *Phys. Chem. Chem. Phys.*, 2019, **21**, 11259–11265.
48 H.-P. Kang, S.-P. Xu, Y.-L. Wang, S.-G. Yu, X.-Y. Zhao, X.-L. Hao, X.-Y. Lai, T. Pfeifer, X.-J. Liu, J. Chen, Y. Cheng and Z.-Z. Xu, *J. Phys. B: At., Mol. Opt. Phys.*, 2018, **51**, 105601.
49 M. Abu-samha and L. B. Madsen, *Phys. Rev. A*, 2020, **102**, 063111.